Solar Phys (2013) 284:77–88
DOI 10.1007/s11207-013-0230-y

Propagation Characteristics of CMEs Associated with Magnetic Clouds and Ejecta

R.-S. Kim · N. Gopalswamy · K.-S. Cho · Y.-J. Moon · S. Yashiro

Received: 6 April 2012 / Accepted: 15 January 2013 / Published online: 5 February 2013

Abstract We have investigated the characteristics of magnetic cloud (MC) and ejecta (EJ) associated coronal mass ejections (CMEs) based on the assumption that all CMEs have a flux rope structure. For this, we used 54 CMEs and their interplanetary counterparts (interplanetary CMEs: ICMEs) that constitute the list of events used by the NASA/LWS Coordinated Data Analysis Workshop (CDAW) on CME flux ropes. We considered the location, angular width, and speed as well as the direction parameter, D. The direction parameter quantifies the degree of asymmetry of the CME shape in coronagraph images, and shows how closely the CME propagation is directed to Earth. For the 54 CDAW events, we found the following properties of the CMEs: i) the average value of D for the 23 MCs (0.62) is larger than that for the 31 EJs (0.49), which indicates that the MC-associated CMEs propagate more directly toward the Earth than the EJ-associated CMEs; ii) comparison between the direction parameter and the source location shows that the majority of the MC-associated CMEs are ejected along the radial direction, while many of the EJ-associated CMEs are ejected non-radially; iii) the mean speed of MC-associated CMEs (946 km s^{-1}) is faster than that of EJ-associated CMEs (771 km s^{-1}). For seven very fast CMEs ($\geq$ 1500 km s^{-1}), all CMEs with large D ($\geq$ 0.4) are associated with MCs and the CMEs with small D are associated with EJs. From the statistical analysis of CME parameters, we found the superiority of the

Flux-Rope Structure of Coronal Mass Ejections
Guest Editors: N. Gopalswamy, T. Nieves-Chinchilla, M. Hidalgo, J. Zhang, and P. Riley

R.-S. Kim (✉) · K.-S. Cho
Korea Astronomy and Space Science Institute, Daejeon, 305-348, Korea
e-mail: rskim@kasi.re.kr

N. Gopalswamy · S. Yashiro
NASA Goddard Space Flight Center, Greenbelt, MD, USA

Y.-J. Moon
School of Space Research, Kyunghee University, Yongin-shi, 446-701, Korea

S. Yashiro
Department of Physics, The Catholic University of America, Washington, DC, USA

direction parameter. Based on these results, we suggest that the CME trajectory essentially determines the observed ICME structure.

Keywords Coronal mass ejections, ejecta · Interplanetary coronal mass ejections, magnetic clouds

1. Introduction

Coronal mass ejections (CMEs) are extremely dynamical events in which closed coronal magnetic field lines are ejected into the interplanetary (IP) space from the Sun (Hundhausen, 1993). When they arrive at the Earth, they are detected as interplanetary CMEs (ICMEs). According to Burlaga *et al.* (1981), ICMEs are classified into two types: magnetic cloud (MC) and ejecta (EJ). An MC is an extension of magnetic flux rope into IP space and defined by above-average magnetic field magnitude, low variance with smooth rotating magnetic field, low plasma beta (ratio of thermal to magnetic pressure), unusual alpha/proton density ratio, and low ion temperature. An MC is a well-structured ICME and about 30 % of ICMEs are MCs (Gosling, 1990). Often, however, identification of an MC can be ambiguous because these characteristics are presented in the literature in various combinations. When the smoothly rotating magnetic field signature is not observed, we refer to the ICME as an EJ (Burlaga *et al.*, 2001).

To understand the ICME structures, several authors have examined the evolution of CME's flux rope structures (Nakwacki *et al.*, 2011; Howard and DeForest, 2012). Numerical simulations show that a flux rope expanding from the solar surface will evolve into an MC with all required plasma characteristics (Roussev *et al.*, 2003; Manchester *et al.*, 2004; Thompson, Kliem, and Török, 2012). According to Gosling (1990), some ICMEs consist of untwisted loops and hence do not show any MC structures. Jacobs *et al.* (2009) successfully simulated a CME with typical characteristics of an MC, but without an underlying helical flux rope structure. On the other hand, Gopalswamy (2006) suggested that all ICMEs have a magnetic flux rope structure, but the passing direction of the spacecraft decides the appearance of ICME as shown in Figure 1. He explained that we can observe an MC only when the observer's trajectory goes through the nose of the magnetic cloud (tracks 3 and 6). In this case, the azimuthal field changes sign at the axis and the magnitude of the azimuthal component also changes, peaking at the axis and falling off on either side. If the spacecraft passes along tracks 4 or 5, the magnetic field will not change and the ICME will be observed as an EJ. It is not clear whether MCs and EJs have intrinsically different structures (flux rope, non-flux rope) or the observed structure is due to different propagation directions. We cannot exclude the possibility of ejected flux ropes being distorted or shredded on their journey from the Sun to the Earth.

Regarding this issue, we are motivated by the proposal of Gopalswamy (2006) that the propagation direction of the CME could be the key to understanding the difference between the two types of ICME. The propagation of CMEs toward the Earth can be investigated using the solar source location and the direction parameter (D) of CMEs. The direction parameter quantifies the degree of asymmetry of the CME shape and shows how closely the CME propagation is directed toward Earth (Moon *et al.*, 2005; Kim *et al.*, 2008). This parameter can be determined directly from coronagraph observations and is applicable to most of the halo CMEs. Note that D is very useful to determine the propagation direction especially for CMEs that are not ejected radially from the source region. In addition, CMEs might experience a distortion of their flux rope structure due to interaction with the background solar wind (Odstrcil and Pizzo, 1999). We expect that the speed of CME could be another important parameter to classify the structure of ICME.

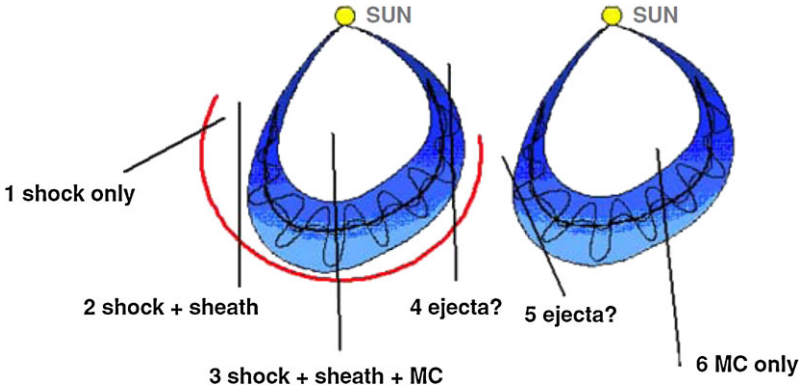

Figure 1 Six possible tracks of an observing spacecraft through an MC with a leading shock (left) and another without (right). Tracks 1 and 2 never encounter the MC proper. Track 3 passes through the nose of the MC. Trajectory 4 passes through the shock, sheath, and through the edge of the MC. Tracks 5 and 6 are similar to 4 and 3, respectively, except that the MC is slow and hence it does not drive a shock. Only trajectories 3 and 6 are expected to observe an MC structure (Gopalswamy, 2006).

In this study, we examined the location, angular width, speed, and the direction parameter of the 54 CDAW events to inspect the different characteristics of MC- and EJ-associated CMEs. We explain our data in Section 2 and present the results in Section 3. Our summary and discussion are given in Section 4.

2. Data

To examine the different characteristics of the CMEs, we used the CDAW list developed for the NASA/LWS Coordinated Data Analysis Workshop (CDAW) on CME flux ropes.[1] The CDAW list contains shock-driving ICMEs during Solar Cycle 23 whose source longitude (l) are located in between E15° and W15°. The list gives us detailed information of the CMEs, which are considered as the sources of ICMEs, and the associated flares. Among the 54 ICMEs, 23 events are classified as MCs (43 %) and 31 events are EJs (57 %). Details of their classification can be found in Gopalswamy *et al.* (2010). From the CDAW list, we used the properties of CMEs, such as the onset date and time, angular width, linear speed, and the location of flare or eruptive prominence for each ICME event.

Adopting the method from Kim *et al.* (2008), we measured the direction parameters, D, for 54 CMEs using the running difference images of the LASCO. For this, we first plotted an ellipse to follow the CME front (see Figure 1 in Kim *et al.*, 2008), and then we drew a line that passes through the centers of both the Sun and the ellipse. The ratio of the shorter to longer distance of the CME front from the solar center along this line is the direction parameter. D is always between 0 and 1, and a larger D indicates a closer orientation toward the Earth. In Table 1, the first three columns are ICME data and the next four columns are related CME data including the direction parameter. The last column is the location of flare or eruptive prominence associated with the ICMEs on the solar surface.

The *Large Angle and Spectrometric Coronagraph* (LASCO: Brueckner *et al.*, 1995) on board the *Solar and Heliospheric Observatory* (SOHO) mission has revealed the various

[1] http://cdaw.gsfc.nasa.gov/meetings/2010_fluxrope/LWS_CDAW2010_ICMEtbl.html.

Table 1 List of shock-driving ICMEs during Solar Cycle 23 (E15° ≤ l ≤ W15°).

CDAW #	ICME		CME				Solar source location
	Type	Start date/time	Onset date/time	Angular width (°)	Speed (km s^{-1})	D	
1	MC	1997/01/10 05:18	01/06 15:10	360	136	0.78	S18E06
2	MC	1997/05/15 09:06	05/12 05:30	360	464	0.78	N21W08
3	EJ	1997/12/11 03:45	12/06 10:27	223	397	0.14	N45W10
4	EJ	1998/05/03 19:00	05/01 23:40	360	585	0.77	S18W05
5	EJ	1998/05/04 10:00	05/02 14:06	360	938	0.58	S15W15
7	EJ	1998/11/07 22:00	11/04 07:54	360	523	0.25	N17W01
8	EJ	1998/11/13 04:30	11/09 18:18	190	325	0.38	N15W05
9	MC	1999/04/16 20:18	04/13 03:30	261	291	0.79	N16E00
10	EJ	1999/06/27 21:30	06/24 13:31	360	975	0.48	N29W13
13	EJ	1999/09/22 21:00	09/20 06:06	360	604	0.95	S20W05
14	EJ	1999/10/21 18:30	10/18 00:06	240	144	0.41	S30E15
15	EJ	2000/01/22 18:00	01/18 17:54	360	739	0.58	S19E11
16	MC	2000/02/21 09:48	02/17 21:30	360	728	0.74	S29E07
17	EJ	2000/07/11 01:30	07/07 10:26	360	453	0.80	N04E00
18	EJ	2000/07/11 22:48	07/08 23:50	161	483	0.13	N18W12
19	MC	2000/07/15 21:06	07/14 10:54	360	1674	0.71	N22W07
20	EJ	2000/07/27 08:28	07/23 05:30	181	631	0.83	S13W05
21	MC	2000/07/28 21:06	07/25 03:30	360	528	0.69	N06W08
23	MC	2000/08/12 06:06	08/09 16:30	360	702	0.73	N20E12
24	MC	2000/09/18 01:54	09/16 05:18	360	1215	0.46	N14W07
25	EJ	2000/10/05 13:13	10/02 03:50	360	525	0.74	S09E07
26	MC	2000/10/13 18:24	10/09 23:50	360	798	0.49	N01W14
27	MC	2000/11/06 23:06	11/03 18:26	360	291	0.79	N02W02
28	EJ	2000/11/27 05:00	11/24 05:30	360	1289	0.57	N20W05
29	EJ	2001/03/04 04:00	02/28 14:50	232	313	0.43	S17W05
30	EJ	2001/03/22 22:30	03/19 05:26	360	389	0.79	S20W00
31	EJ	2001/04/11 22:30	04/09 15:54	360	1192	0.69	S21W04
32	MC	2001/04/12 07:54	04/10 05:30	360	2411	0.49	S23W09
33	MC	2001/04/29 01:54	04/26 12:30	360	1006	0.30	N20W05
34	EJ	2001/08/13 07:00	08/09 10:30	175	479	0.33	N11W14
35	EJ	2001/10/12 03:30	10/09 11:30	360	973	0.53	S28E08
36	MC	2002/03/19 22:54	03/15 23:06	360	957	0.61	S08W03
37	MC	2002/04/18 04:18	04/15 03:50	360	720	0.86	S15W01
38	EJ	2002/05/11 13:00	05/08 13:50	360	614	0.67	S12W07
39	MC	2002/05/19 03:54	05/16 00:50	360	600	0.41	S23E15
40	EJ	2002/05/20 11:00	05/17 01:27	45	461	0.19	S20E14
41	EJ	2002/05/30 07:09	05/27 13:27	161	1106	0.12	N22E15
42	EJ	2002/07/18 12:00	07/15 21:30	188	1300	0.39	N19W01
43	MC	2002/08/01 11:54	07/29 12:07	161	222	0.75	S10W10
44	MC	2003/08/18 11:36	08/14 20:06	360	378	0.44	S10E02
45	MC	2003/10/29 08:00	10/28 11:30	360	2459	0.94	S16E08

Table 1 (*Continued*)

CDAW #	ICME		CME				Solar source location
	Type	Start date/time	Onset date/time	Angular width (°)	Speed (km s^{-1})	D	
46	MC	2003/10/31 02:00	10/29 20:54	360	2029	0.83	S15W02
47	EJ	2004/01/22 08:00	01/20 00:06	360	965	0.76	S13W09
48	MC	2004/07/24 12:48	07/22 08:30	132	899	0.01	N04E10
49	MC	2004/11/09 20:54	11/06 02:06	214	1111	0.72	N09E05
50	EJ	2004/12/12 12:00	12/08 20:26	360	611	0.73	N05W03
51	EJ	2005/01/16 14:00	01/15 06:30	360	2049	0.07	N16E04
52	EJ	2005/02/18 15:00	02/13 11:06	151	584	0.13	S11E09
53	MC	2005/05/15 05:42	05/13 17:12	360	1689	0.79	N12E11
54	MC	2005/05/20 07:18	05/17 03:26	273	449	0.21	S15W00
56	EJ	2005/07/10 10:30	07/07 17:06	360	683	0.16	N09E03
57	EJ	2005/09/02 19:03	08/31 11:30	360	825	0.69	N13W13
58	EJ	2005/09/15 14:24	09/13 20:00	360	1866	0.31	S09E10
59	EJ	2006/08/20 00:00	08/16 16:30	360	888	0.44	S16W08

shapes of CMEs as shown in Figure 2(a) and (c). The CME observed on 28 October 2003 (CDAW #45) was associated with a strong X-ray flare (X17.2) at S16E08, and observed as a symmetric halo with a speed of 2456 km s^{-1} (Gopalswamy *et al.*, 2005; see Figure 2(a)). This CME was detected as an MC when it arrived at the Earth on 29 October 2003 as shown in Figure 2(b). The figure shows a smoothly rotating and increasing magnetic field, which is an indicator of MC. Another CME observed on 15 January 2005 (CDAW #51) was associated with an M8.6 class flare from N16E04 as shown in Figure 2(c). It was also a halo event with high speed (2049 km s^{-1}) from the solar center. In this case, the CME turned into an EJ when observed by *in-situ* spacecraft on 16 January 2005 (Figure 2(d)). As shown in the figure, there was no distinct rotation of magnetic field and the strength remained less than 10 nT during the passage of the EJ. The direction parameters for these two events were compiled as 0.94 (28 October 2003) and 0.07 (15 January 2005). The northward bias of the latter event resulted in a smaller D.

3. Results

3.1. Source Location and Angular Width

Since we have already selected only the CMEs with source regions close to the solar center, it is clear that both MCs and EJs originate near the central meridian as listed in Table 1. The distribution of source locations for the 54 CMEs in Figure 3(a) shows that the mean longitude ($|l|$) for the 23 MCs is 6.6°, which is similar to that for 31 EJs (7.6°). As shown in the figure, there is no significant difference between the source locations for MCs and EJs. The p value of the T test for two groups of MC and EJ is 0.199, which is much higher than the significance level (0.05).

The distribution of angular widths of the CMEs in Figure 3(b) shows that a large portion (38/54, 70 %) of the 54 CMEs are full halos (AW = 360°) with the mean angular width

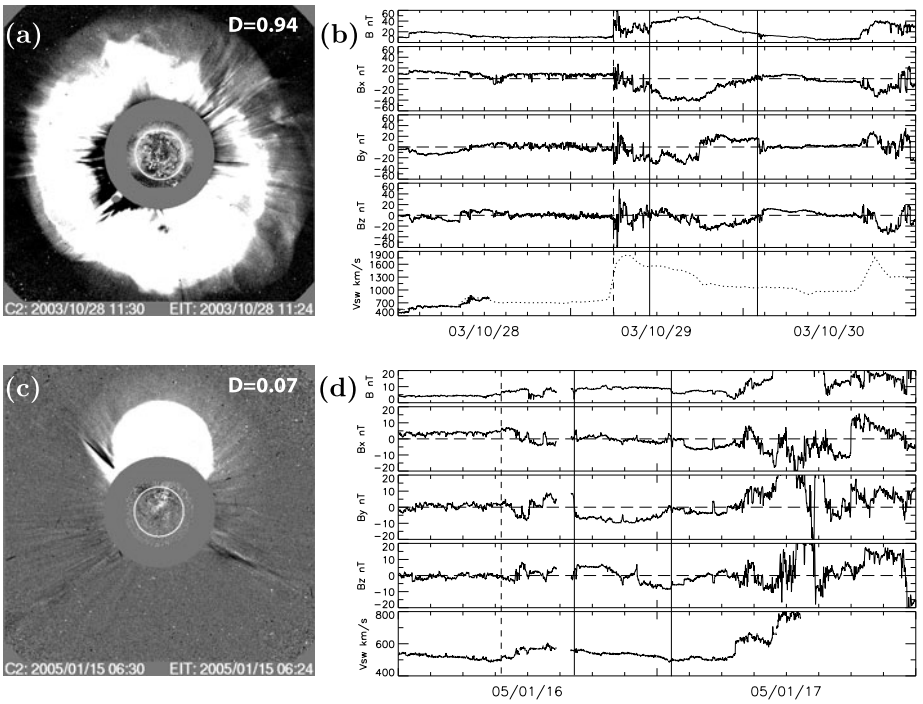

Figure 2 LASCO C2 running difference images for the CMEs on 28 October 2003 (a) and on 15 January 2005 (c). (b) and (d) show the time profiles of magnetic field intensity, B_X, B_y, B_z components in geocentric solar ecliptic (GSE) coordinates, and the solar wind bulk velocity observed by the *Solar Wind Electron, Proton, and Alpha Monitor* (SWEPAM) on board the *Advanced Composition Explorer* (ACE; Gloeckler *et al.*, 1998). We also use the data from the *Solar Wind Ion Composition Spectrometer* (SWICS) on board the ACE when the SWEPAM does not give solar wind parameters because the speed is too high, as represented by dotted line (b). The start time of IP shock and the boundaries of ICME are denoted by vertical dashed (shock) and solid lines (ICME).

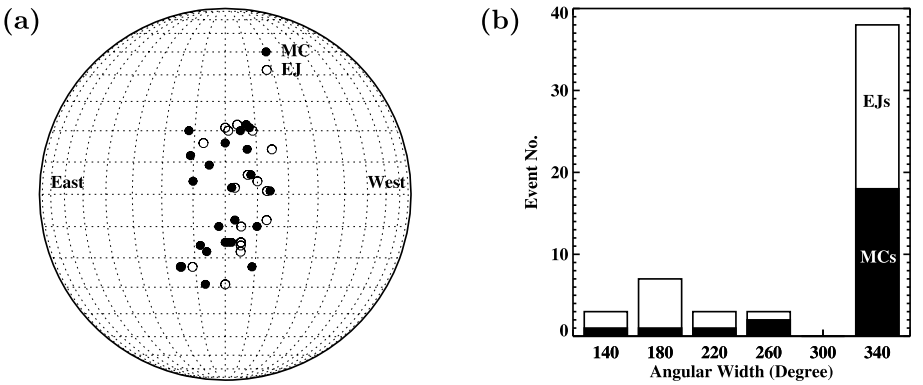

Figure 3 Distribution of the source region locations (a) and the angular width (b) of MC and EJ events.

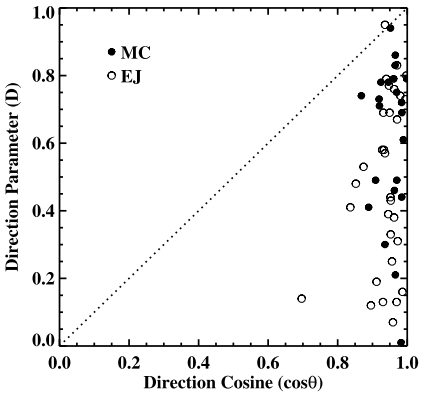

Figure 4 The relationship between the direction cosine of the CME source location and the direction parameter. The filled and empty circles represent MCs and EJs, respectively.

of 309°. Among the halos, there are 18 MC-associated CMEs and 20 EJ-associated CMEs. Among the 16 non-halo CMEs, five events are MC-associated CMEs and 11 events are EJ-associated CMEs. The mean angular widths for MC and EJ are 327° and 295°, respectively. We found that there is no big difference between them in the angular width distribution because the majority of CMEs in the two groups are full halo events.

3.2. Direction Parameter

The source locations of the two events in Figure 2 have similar distances from the solar center (S16E08 and N16E04), but they show different ICME structures; one is detected as an MC and the other an EJ. This is a typical example showing a possibility that even though all events occurred near the solar center, their propagation directions might be different, leading to different ICME structures at 1 AU. Thus, we inspected the propagation direction using D for all the events in the CDAW list. Recall that the 28 October 2003 CME has a large D (0.94), but the one on 15 January 2005 has a small D (0.07).

To verify the hypothesis that the propagation directions of CMEs might be different even though they originate from the vicinity of the central median on the Sun, we examined the relation between the source locations and the propagation directions for 54 CDAW events, supposing that CMEs propagate radially. In Figure 4, we compare D with the direction cosine, $\cos\theta$, where θ is the angular distance of the source region from the solar center. The direction cosine is between 0 to 1 and it should be 1 when the source location is exactly at the solar center. For the 54 CDAW events, we found that $\cos\theta$ occupies a narrow range $(0.8-1)$ except for one event as shown in the figure (mean $= 0.94$), while D is randomly scattered over the entire range (mean $= 0.54$). If all CMEs are ejected radially, these two values should be similar for each event. In this case, the events should fall near the dotted line in the figure, but the distribution in the figure deviates significantly from the dotted line. This result shows that many of the CMEs are not ejected along the radial direction and their noses may not reach the Earth even though they are ejected from the vicinity of the center of the solar disk.

We also examined the dependence of D on the ICME type: MC and EJ. The average D values for 23 MCs and 31 EJs are 0.62 and 0.49, respectively. These values are relatively high, since the CDAW events are from the disk center. However, EJ's D value is only slightly higher ($+0.06$) than the average D for the 486 halo CMEs ($D = 0.43$; Kim *et al.*, 2008), in spite of the data set from the disk center. Please note that MC's D value is almost 1.5 times of that for entire sample of halo CMEs. Figure 5(a) and (b) show that Ds for MC-associated

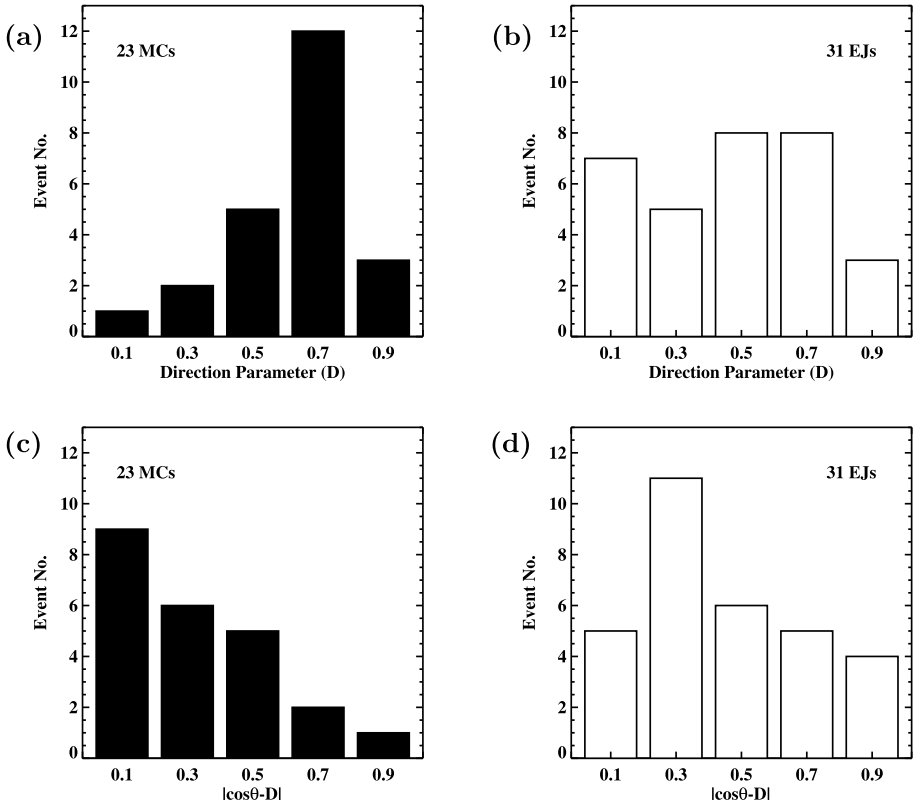

Figure 5 The distributions of the direction parameter for MC and EJ events (a and b) and the amount of deflection of MC and EJ events (c and d).

CMEs follow a Gaussian distribution with the median value of 0.72, while those of EJ-associated CMEs are evenly spread (median = 0.48). The p value of the T test between the two groups is 0.048 (< 0.05), which means that the difference is statistically significant.

We also examined the difference between $\cos\theta$ and D ($|\cos\theta - D|$) for each event as shown in Figure 5(c) and (d). This value can be regarded as a proxy of the CME deflection from the radial direction. We found that the majority of MC-associated CMEs are not deflected much with peak difference between 0 and 0.2 as shown in Figure 5(c). On the other hand, many of EJs show some deflection with peak value between 0.2 and 0.4 in Figure 5(d). This result suggests a tendency in our dataset that EJs either erupt non-radially or experience more deflection than MCs.

3.3. CME Speed

The association between the CMEs and MCs can be explained by the direction parameter, but the association between the CMEs and EJs is difficult to explain with the direction parameter as shown in Figure 5(a) and (b). To inspect other effects on the EJ-associated CMEs, we considered the linear speed of CMEs and examined the combined effect of the speed and direction parameter. In Figure 6(a) and (b), we can see a tendency that slow CMEs are more likely to be associated with EJs. Of the 31 EJ-associated CMEs, 25 have

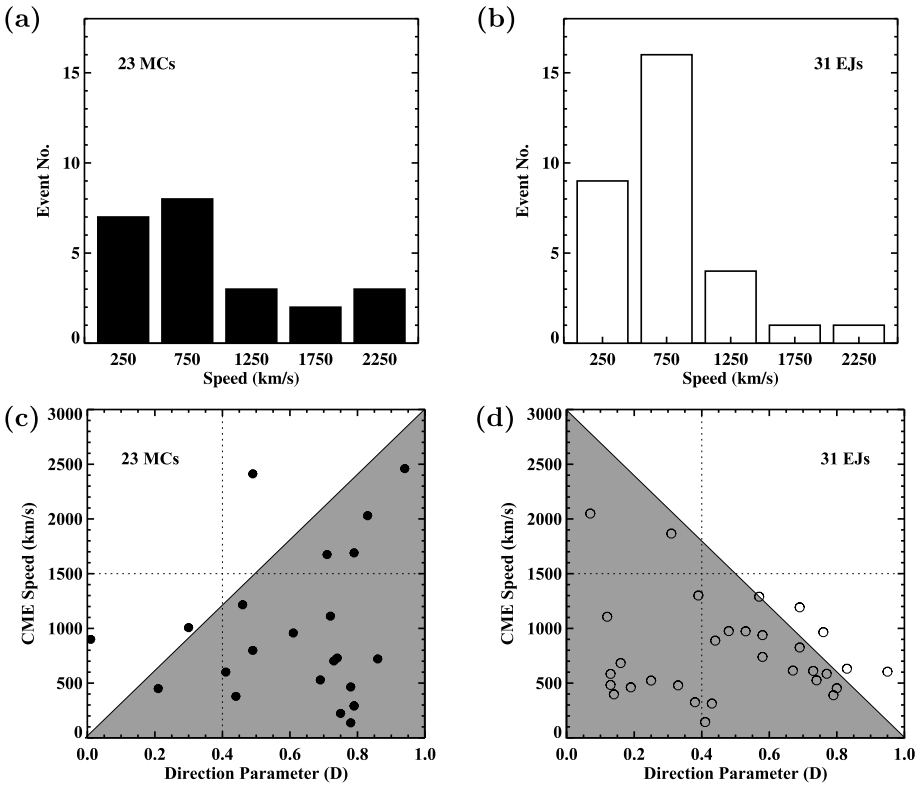

Figure 6 Associated CME speed for MCs (a) and EJs (b), and the distribution of MCs (c) and EJs (d) as a function of the speed and the direction parameter. The horizontal dotted lines indicate $V = 1500$ km s^{-1} and the vertical dotted lines indicate $D = 0.4$.

lower speeds than 1000 km s^{-1} (81 %), while the 23 MC-associated CMEs do not show any strong dependences as the EJs-associated CMEs do. The mean speed for the CDAW events is 846 km s^{-1} and those for MC- and EJ-associated CMEs are 946 km s^{-1} and 771 km s^{-1}, respectively.

Although the difference in mean speed is not statistically significant (p value $= 0.253$), we can find a combined effect of speed and direction parameter as shown in Figure 6(c) and (d). The majority of the MCs are located beneath the increasing diagonal line (increasing speed with D) and a large portion of the EJs are located beneath the decreasing diagonal line (decreasing speed with D) as shown in the gray portions of Figure 6(c) and (d), respectively. This result implies that, for the faster CME, D is more important to classify the ICME. This becomes clearer in the case of seven very fast CMEs (≥ 1500 km s^{-1}), since all large-D events (≥ 0.4) are MCs, and all small-D events are EJs.

Contrary to our result, Gopalswamy *et al.* (2010) reported that the MC-associated CMEs have lower speeds than EJ-associated CMEs using 222 IP shock–CME pairs. They explained that the difference in CME speeds stem from the fact that the MC-associated CMEs mostly originate close to the disk center, and the EJ-associated CMEs originate at intermediate central meridian distances. Then MC-associated CMEs are more subject to projection effects than EJ-associated CMEs. However, since our data set is selected from the central events,

Table 2 Definition of verification statistics.

	Observed MC	Observed EJ	Total
Predicted MC	hit (a)	false (b)	a + b
Predicted EJ	miss (c)	null (d)	c + d
Total	a + c	b + d	a + b + c + d
Probability of detection, yes (PODy)			a/(a + c)
Probability of detection, no (PODn)			d/(b + d)
Critical success index (CSI)			a/(a + b + c)

Table 3 Three contingency tables with criteria of the average values of 486 halo CMEs (Kim *et al.*, 2008).

CME parameters				PODy	PODn	CSI	χ^2 (p value)
$\cos\theta = 0.7$	MC	EJ	Total				
Inner	23	30	53	1.00	0.03	0.43	0.76 (0.385)
Outer	0	1	1				
Total	23	31	54				
$D = 0.4$	MC	EJ	Total				
Large D	20	19	39	0.87	0.39	0.48	4.34 (0.037)
Small D	3	12	15				
Total	23	31	54				
$V = 800$ km s^{-1}	MC	EJ	Total				
Fast	10	12	22	0.43	0.61	0.29	0.12 (0.724)
Slow	13	19	32				
Total	23	31	54				

even the EJ-associated CMEs cannot avoid the projection effects. Therefore, our result is in line with the result of Gopalswamy *et al.* (2010).

3.4. Statistical Significance

To evaluate the capability of ICME classification using the CME parameters, we adopted a contingency table that has been widely used in the meteorological forecasting literature. Table 2 is a general form of the contingency table, which provides us with the information of the success or failure (or degree thereof) of the forecasting experience in real time (Smith *et al.*, 2000). In this table, the 'hit' means correctly predicted for an MC. The 'false' means predicted for an MC, but observed as an EJ. Similarly, the 'miss' is predicted for an EJ, but observed as an MC, and the 'null' is correctly predicted for an EJ. The statistics, such as the probability of detection 'yes' (PODy) and the critical success index (CSI), may then be computed as shown in the table. CSI ranges from 0 to 1, with a value of 1 indicating a perfect forecast.

Table 3 shows three 2 × 2 contingency tables based on the CME location, direction parameter, and speed. As the criteria for parameters, we applied 0.7 for $\cos\theta$, 0.4 for D, and 800 km s^{-1} for speed based on the average values of the 486 general halo CMEs (Kim *et al.*,

2008). If an event has larger value than each criterion, we expect the ICME as an MC, otherwise as an EJ. Since the data set already selected the events from the central meridian, almost all CMEs are so biased inner events that we cannot discern MC or EJ using their location as shown in the first contingency table. In this case, PODy, PODn, and CSI are estimated to be 1.00, 0.03, and 0.43, respectively. Similarly, it also seems hard to classify CME into MC or EJ using only the speed of CME. The events are evenly distributed in each cell as shown in the third contingency table. PODy, PODn, and CSI are estimated to be 0.43, 0.61, and 0.29, respectively. The p values from χ^2 test of the directional cosine and the speed are 0.385 and 0.724, respectively. These values are too high to have any significance on the classification of the ICME. In contrast, the direction parameter can provide reliable classification with sufficient statistical significance (p value $= 0.037$). As shown in the second contingency table, its PODy, PODn, and CSI are estimated to be 0.87, 0.39, and 0.48, respectively.

4. Summary and Discussion

We examined the CME parameters to check whether all the CMEs have flux rope structure using the 54 CME–ICME pairs compiled for the NASA/LWS Coordinated Data Analysis Workshop. We did not find any significant difference between 23 MCs and 31 EJs from the comparison of their source locations and angular widths. The average value of D for MC events (0.62) is larger than that for EJ events (0.49). We found a tendency that the EJ-associated CMEs are ejected non-radially or experience deflections more than the MC-associated CMEs. Regarding the CME speed, the mean value for MCs is 946 km s^{-1} and that for EJs is 771 km s^{-1}. Among the 31 EJs, 25 events have low CME speeds (< 1000 km s^{-1}, 81 %), while the MCs have less slow CMEs (15/23, 65 %, *cf.* the fraction of slow CME from Kim *et al.* (2008) is 72 %). We also examined the combined effect of the direction parameter and speed. It is found that the majority of the MCs have large D (≥ 0.4) and the majority of the EJs have slow speed (< 1500 km s^{-1}). This result can be summarized that EJ-associated CMEs have slow speeds, and MC-associated CMEs have large D. We also found a clear tendency in the case of seven very fast CMEs (≥ 1500 km s^{-1}) that all large-D events (≥ 0.4) are MCs, and all small-D events are EJs.

Our study is a simple analysis, but it provides a clue to answer the question whether all CME have flux rope structure. If we use only the CME source information to classify ICMEs, it seems hard to find any differences between MCs and EJs. However, if we use the CME propagation direction and speed, we can find a hint for the answer. Based on our results, we suggest that some of the CMEs are not ejected along the radial direction and they may not reach the Earth by their noses. In this case, we may not detect the flux rope structure even if they have one. Our result is consistent with those by Xie, Gopalswamy, and Cyr (2013), who reported that the EJ-associated CMEs were deflected more away from the disk center, while the MC-associated CMEs were deflected more towards the disk center using the Krall flux rope model. Our result is also consistent with those by Mäkelä *et al.* (2013) who found that the EJ-associated CMEs are prone to deflection by nearby coronal holes.

If the CMEs associated with MCs and EJs have originally different flux rope structures, they should be observed differently without no dependence on the CME speed. However, our observation shows that slow CMEs are more likely to be EJs than fast CMEs, and fast CMEs are to be EJs, only when they have small Ds. Based on the above results, we suggest that all CMEs have a flux rope structure and the trajectory of the CMEs essentially decides the observed ICME structure.

Acknowledgements This work benefited from the NASA/LWS Coordinated Data Analysis Workshops on CME flux ropes in 2010 and 2011. We acknowledge the workshop support provided by NASA/LWS, Predictive Sciences, Inc. (San Diego, CA), University of Alcala (Alcala de Henares, Spain), and Ministerio de Ciencia e Innovacion (Reference number AYA2010-12439-E), Spain. This work was partially supported by the Construction of Korean Space Weather Center as the project of KASI, the KASI Basic Research Fund, and Research Fellowship for Young Scientists of KRCF. Y.-J.M. has been supported by the WCU program (No. R31-10016) and Basic Research Promotion Fund (20090071744 and 20100014501) through the National Research Foundation of Korea funded by the Ministry of Education, Science and Technology.

References

Brueckner, G.E., Howard, R.A., Koomen, M.J., Korendyke, C.M., Michels, D.J., Moses, J.D., *et al.*: 1995, The Large Angle Spectroscopic Coronagraph (LASCO). *Solar Phys.* **162**, 357.

Burlaga, L.F., Sittler, E., Mariani, F., Schwenn, R.: 1981, Magnetic loop behind an interplanetary shock: *Voyager*, *Helios*, and IMP 8 observations. *J. Geophys. Res.* **86**, 6673.

Burlaga, L.F., Skoug, R.M., Smith, C.W., Webb, D.F., Zurbuchen, T.H., Reinard, R.: 2001, Fast ejecta during the ascending phase of solar cycle 23: ACE observations, 1998 – 1999. *J. Geophys. Res.* **106**(A10), 20957.

Gloeckler, G., Cain, J., Ipavich, F.M., Tums, E.O., Bedini, P., Fisk, L.A., *et al.*: 1998, Investigation of the composition of solar and interstellar matter using solar wind and pickup ion measurements with SWICS and SWIMS on the ACE spacecraft. *Space Sci. Rev.* **86**, 497.

Gopalswamy, N.: 2006, Properties of interplanetary coronal mass ejections. *Space Sci. Rev.* **124**, 145.

Gopalswamy, N., Yashiro, S., Liu, Y., Michalek, G., Vourlidas, A., Kaiser, M.L., Howard, R.A.: 2005, Coronal mass ejections and other extreme characteristics of the 2003 October – November solar eruptions. *J. Geophys. Res.* **110**, A09S15. doi:10.1029/2004JA010958.

Gopalswamy, N., Xie, H., Mäkelä, P., Akiyama, S., Yashiro, S., Kaiser, M.K., Howard, R.A., Bougeret, J.-L.: 2010, Interplanetary shocks lacking type II radio burst. *Astrophys. J.* **710**, 1111.

Gosling, J.T.: 1990, In: *Physics of Magnetic Flux Ropes*, *Geophys. Monogr. Ser.* **58**, AGU, Washington, 343.

Howard, T.A., DeForest, C.E.: 2012, Inner heliospheric flux rope evolution via imaging of coronal mass ejection. *Astrophys. J.* **746**, 64.

Hundhausen, A.J.: 1993, Size and locations of coronal mass ejections – SMM observations from 1980 and 1984 – 1989. *J. Geophys. Res.* **98**(A8), 13177.

Jacobs, C., Roussev, I.I., Lugaz, N., Poedts, S.: 2009, The internal structure of coronal mass ejections: are all regular magnetic clouds flux ropes? *Astrophys. J. Lett.* **695**, L171.

Kim, R.-S., Cho, K.-S., Moon, Y.-J., Dryer, M., Yi, Y., Lee, J., Kim, K.-H., Wang, H., Song, H., Park, Y.-D.: 2008, CME earthward direction as an important geoeffectiveness indicator. *Astrophys. J.* **677**, 1378.

Mäkelä, P., Gopalswamy, N., Xie, H., Mohamed, A.A., Akiyama, S., Yashiro, S.: 2013, Coronal hole influence on the observed structure of interplanetary CMEs. *Solar Phys.*, in this issue. doi:10.1007/s11207-012-0211-6.

Manchester, W.B., Gombosi, T.I., Roussev, I., DeZeeuw, D.L., Sokolov, I.V., Powell, K.G., Tóth, G., Opher, M.: 2004, Three-dimensional MHD simulation of a flux rope driven CME. *J. Geophys. Res.* **109**(A1), A01102.

Moon, Y.-J., Cho, K.-S., Dryer, M., Kim, Y.-H., Bong, S.-C., Chae, J., Park, Y.D.: 2005, New geoeffective parameters of very fast halo coronal mass ejections. *Astrophys. J.* **624**, 414.

Nakwacki, M.S., Dasso, S., Démoulin, P., Mandrini, C.H., Gulisano, A.M.: 2011, Dynamical evolution of a magnetic cloud from the Sun to 5.4 AU. *Astron. Astrophys.* **535**, 52.

Odstrcil, D., Pizzo, V.J.: 1999, Distortion of the interplanetary magnetic field by three-dimensional propagation of coronal mass ejections in a structured solar wind. *J. Geophys. Res.* **104**(A12), 28225.

Roussev, I.I., Gombosi, T.I., Sokolov, I.V., Velli, M., Manchester, W., DeZeeuw, D.L. IV, *et al.*: 2003, A three-dimensional model of the solar wind incorporating solar magnetogram observations. *Astrophys. J. Lett.* **595**, L57.

Smith, Z., Dryer, M., Ort, E., Murtagh, W.: 2000, Performance of interplanetary shock prediction model: STOA and ISPM. *J. Atmos. Solar-Terr. Phys.* **62**, 1265.

Thompson, W.T., Kliem, B., Török, T.: 2012, 3D reconstruction of a rotating erupting prominence. *Solar Phys.* **276**, 241.

Xie, H., Gopalswamy, N., St. Cyr, O.C.: 2013, Near-Sun flux rope structure of CMEs. *Solar Phys.*, in this issue. doi:10.1007/s11207-012-0209-0.